phys. stat. sol. (a) **205**, No. 5, 1093–1095 (2008) / **DOI** 10.1002/pssa.200778468

physica status solidi a
www.pss-a.com
applications and materials science

Electro-optical intersubband modulators at telecommunication wavelengths based on GaN/AlN quantum wells

N. Kheirodin[1], L. Nevou[1], H. Machhadani[1], M. Tchernycheva[*,1], A. Lupu[1], F. H. Julien[1], P. Crozat[1], L. Meignien[1], E. Warde[1], L. Vivien[1], G. Pozzovivo[2], S. Golka[2], G. Strasser[2], F. Guillot[3], E. Monroy[3], T. Remmele[4], and M. Albrecht[4]

[1] Institut d'Electronique Fondamentale, UMR 8622 CNRS, Bat. 220, Université Paris-Sud, 91405 Orsay, France
[2] Zentrum für Mikro- und Nanostrukturen, Technische Universität Wien, Floragasse 7, 1040 Vienna, Austria
[3] Equipe mixte CEA-CNRS-UJF Nanophysique et Semiconducteurs, DRFMC/SP2M/PSC, CEA-Grenoble, 17 Rue des Martyrs, 38054 Grenoble Cedex 9, France
[4] Institut für Kristallzüchtung, Max-Born-Straße 2, 12489 Berlin, Germany

Received 5 September 2007, revised 20 March 2008, accepted 20 March 2008
Published online 23 April 2008

PACS 42.79.Hp, 73.63.Hs, 78.67.De, 85.35.Be, 85.60.Bt

[*] Corresponding author: e-mail maria.tchernycheva@ief.u-psud.fr, Phone: +33169154051, Fax: +33169154115

We report the demonstration of intersubband modulators operating at telecommunication wavelengths at room temperature based on GaN/AlN quantum wells. We first investigate electro-optical modulators making use of electron tunneling in coupled quantum wells. Electro-absorption modulation with opposite sign induced by the electron tunneling between the reservoir and active quantum wells is observed at $\lambda = 1.3-1.6$ μm and $\lambda = 2.2$ μm. We show that by reducing the mesa size down to 15×15 μm^2, optical modulation bandwidth as large as 3 GHz can be obtained. We then investigate waveguide intersubband modulators relying on the depletion of the ground electronic state of a 3 quantum well active region. Modulation depths as large as 14 dB in the wavelength range of 1.2–1.6 μm are obtained under –9 V/+7 V voltage swing.

1 Introduction III-nitride materials are well known for their optoelectronic applications in the visible–UV spectral range. They also offer prospects for ultrafast optoelectronic devices at fiber-optics telecommunication wavelengths based on intersubband (ISB) transitions in quantum well (QW) heterostructures. III-nitride ISB devices have the potential for ultrafast operation because the absorption recovery time is extremely short in the 0.15–0.4 ps range due to enhanced electron-LO phonon scattering. Ultrafast optical switches, high frequency ISB photodetectors at $\lambda = 1.3-1.55$ μm, as well as ISB light emitting devices have been recently demonstrated [1–3]. The coupling between GaN/AlN QWs has also been studied [4]. Electro-optical modulators based on Stark shift of the ISB absorption with frequency response as high as 60 GHz have been proposed [5]. Experimentally, nitride ISB modulators relying on bias control of the electron population of a surface superlattice have been demonstrated [6].

In this paper, we report on high-speed high-efficiency electro-optical modulators at telecommunication wavelengths based on GaN/AlN QWs. Two kinds of devices are investigated. The first series relies on bias-controlled electron tunneling in coupled quantum wells (CQW) [7]. The devices exhibit multi-GHz optical modulation bandwidth at room temperature. The second series are waveguide-based GaN/AlN QW modulators relying on bias controlled electron depletion/population of the ground state. Modulation depth as large as 14 dB is demonstrated at telecommunication wavelengths.

2 Coupled quantum well modulators The active structure of the CQW modulator consists of a wide well, which acts as an electron reservoir, and of a narrow well designed to exhibit ISB absorption at 1.3 μm. The operation principle is sketched in Fig. 1. By applying a positive bias on the CQW structure, electrons are transferred from

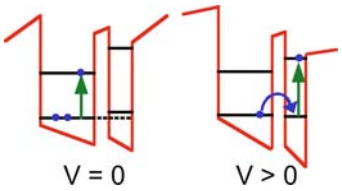

Figure 1 (online colour at: www.pss-a.com) Operation principle of CQW modulator.

the reservoir well to the active well, which gives rise to electro-absorption at $\lambda = 1.3-1.6$ μm.

The samples were grown by plasma-assisted molecular beam epitaxy on AlN-on-sapphire templates. The substrate temperature was fixed to 720 °C, and the growth rate was 0.28 ML/s, determined by the nitrogen supply. The active region contains 20 periods of CQWs separated by 2.7 nm thick AlN spacer layers. The CQWs consist of a 3 nm thick GaN reservoir well, a 1 nm thick AlN coupling barrier, and a 1 nm thick GaN well n-doped with silicon at 5×10^{19} cm^{-3}. The active region is sandwiched between two $Al_{0.6}Ga_{0.4}N$ layers n-doped with silicon at 5×10^{19} cm^{-3}, which serve as bottom and top contacts with respective thicknesses of 500 and 125 nm.

Reactive ion etching with chlorine gas was used to etch square mesas down to the bottom contact layers. The mesa size ranges from 15×15 μm^2 up to 700×700 μm^2. A Ti/Al/Ti/Au metallization was performed on the bottom $Al_{0.6}Ga_{0.4}N$ contact layer followed by annealing at 750 °C during 30 s. Another Ti/Au metallization was then carried out to form a Schottky contact on the top contact layer. As shown in the inset of Fig. 2, the top contacts have an open-square geometry in order to allow optical testing of the devices at Brewster's angle of incidence.

Infrared absorption measurements were performed at room temperature using a Fourier Transform Infrared (FTIR) spectrometer and an InGaAs photodiode with a cut-off wavelength of 2.6 μm. The absorption spectrum for p-polarized light shows a peak at 0.56 eV with a full width at half maximum (FWHM) of 85 meV ascribed to the ISB absorption of the reservoir well as well as a broader peak at 0.9 eV (FWHM 105 meV) ascribed to the ISB absorption of the active well. From these measurements, we estimate that the ground state of the active well is only 28 meV above that of the reservoir well.

Electron tunneling between the wells was probed at room temperature by measuring the ISB absorption at Brewster's angle of incidence versus applied bias with a FTIR spectrometer. The phase and magnitude of the transmission change, $\Delta T/T$, was calibrated at a wavelength of 1.34 μm using irradiation by a continuous-wave $Nd:YVO_4$ laser. Figure 2 shows the differential modulation for various positive and negative bias pulses for a 700×700 μm size mesa. With increasing positive bias, electrons are transferred from the reservoir well to the active well and the ISB absorption at $\lambda = 2.2$ μm decreases, while the absorption in the wavelength range of 1.2–1.67 μm increases. An opposite behavior is observed

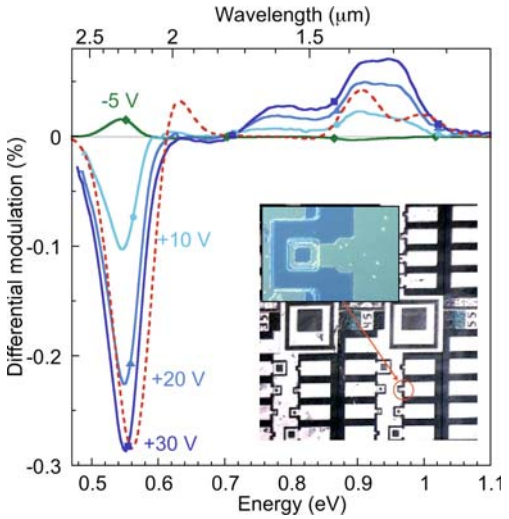

Figure 2 (online colour at: www.pss-a.com) Differential modulation, $-\Delta T/T$, spectrum for applied bias pulses of +30 V (squares), +20 V (triangles), +10 V (circles), and −5 V (diamonds). The dashed line shows the calculated transmission change for 0.8 V bias voltage across the active region. Inset: Top view image of 270×270, 90×90, 50×50, 30×30 and 15×15 μm^2 mesas.

for negative bias. This is a clear signature that the absorption modulation arises from charge transfer between the two wells. It should be noted that, because of the rather large contact resistance, an applied bias of 30 V corresponds to 0.8 V across the active CQW region.

The modulation depth was measured at 1.34 μm wavelength using a $Nd:YVO_4$ laser with an incidence angle of 45°. The modulation depth is 30% for the 30×30 μm^2 mesas under 10 V bias. It increases when reducing the mesa size. Indeed, for smaller mesas the electric field at the center of the top contact is expected to be stronger when the distance to the metal contact is shorter.

The frequency response of the modulators was measured at $\lambda = 1.34$ μm by focusing the $Nd:YVO_4$ laser at 45° angle of incidence onto the hollow top contact. A RF waveform synthesizer was used to bias the devices at 13 dBm electrical power. In order to eliminate the pick-up noise, the transmitted light was coupled into a 10 m long optical fiber and remotely detected by an InGaAs photodiode with a −3 dB frequency response of 32 GHz and a spectrum analyzer. The mesas were bonded with 8 mm long gold wires to a SMA connector. The inset of Fig. 3 shows the frequency response of the various modulators at room temperature. The optical modulation bandwidth – which corresponds to −6 dB electrical signal bandwidth – as a function of mesa size is shown in Fig. 3. The optical modulation bandwidth increases when reducing the mesa size and reaches 3 GHz for the 15×15 μm^2 mesas. As seen there is a clear benefit of the device miniaturization in terms of increased modulation bandwidth.

In order to investigate the main factors governing the device speed, we used a 20 GHz network analyzer to

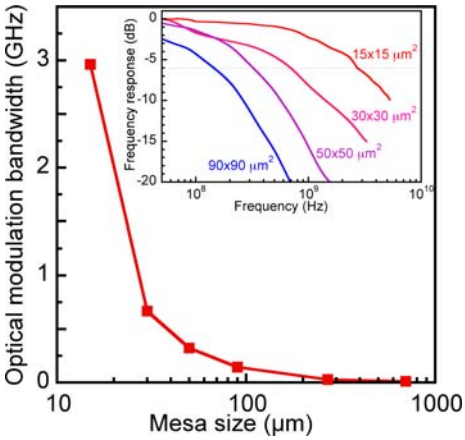

Figure 3 (online colour at: www.pss-a.com) Optical modulation bandwidth at 1.34 μm wavelength versus mesa size. The inset shows the frequency response of the various mesa devices.

measure the S-parameters of the various mesa devices. For mesa sizes above 30 μm, the modulation bandwidth is found to be limited by the RC time constant due to the resistance of the contacts and the device capacitance. This is not the case for the smaller 15 μm mesas, because the frequency response due to the 50 Ω line resistor and device parasitic capacitance in that case is comparable to that due to the inherent R and C of device. This means that further reduction of the device size will not improve the modulation bandwidth unless reducing the parasitic capacitance, which can be achieved by implementing dedicated RF 50 Ω access lines for the top and bottom contacts. In terms of intrinsic speed, the CQW modulator is limited by the electron tunneling time through the 1 nm thick AlN barrier which is estimated to be in the 1–5 ps range, which corresponds to >30 GHz modulation bandwidth. In order to further increase the frequency response while providing a reduction of the driving voltage, the access resistance must be decreased. This can be obtained by reducing the Al content of the Si-doped contact layers.

3 Waveguide-based modulators The principle of operation of the waveguide depletion modulator is similar to that of Ref. [6]. Under negative applied bias, the QWs are depleted and the modulator is transparent, while under positive applied bias the electron population of the ground state of the wells gives rise to ISB absorption at 1.5 μm wavelength.

The sample was grown by plasma-assisted molecular beam epitaxy on a 1 μm thick AlN-on-sapphire template. It consists of 3 periods of 1.3 nm thick GaN wells with 3 nm thick AlN barriers. The wells are n-doped with Si at 2×10^{19} cm^{-3}. The active region is sandwiched between two 500 nm $Al_{0.5}Ga_{0.5}N$ contact layers n-doped with Si at 5×10^{18} cm^{-3} which acts as bottom and top waveguide cladding layers. Etching is used to fabricate 50 μm wide ridge waveguides with a length of 1.675 mm. Metal is then deposited to form the top and bottom contacts.

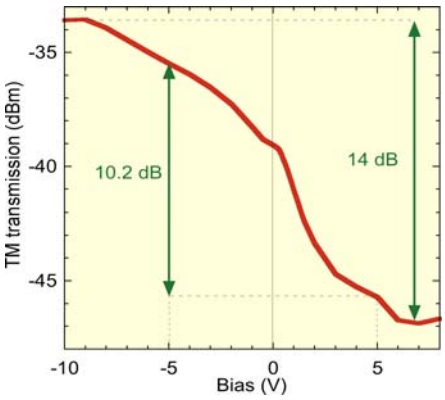

Figure 4 (online colour at: www.pss-a.com) Transmission of the modulator versus static applied bias for TM-polarization.

Figure 4 shows the room-temperature transmission for TM polarization of one of the waveguide devices versus the static applied bias. We used a broadband super luminescent diode ($\lambda = 1.4–1.6$ μm) and a lensed fiber for the measurements. The transmission rapidly decreases between –9 V and 7 V as a consequence of the increased ISB absorption resulting from the electron population of the QWs. For TE polarization the transmission (–26 dBm) does not depend on applied bias (not shown in the figure). As displayed in Fig. 4, the modulation depth is very large, of the order of 14 dB for –9 V/+7 V applied bias and 10 dB for ±5 V voltage swing. It should be noted that a value of 12 dB is required for optical modulators in order to achieve 10^{-12} bit error rates in current technology fiber-optics data transmission systems.

Acknowledgements The AlN-on-sapphire templates were gently supplied by DOWA Instruments. Financial support by European FP6 NitWave program (contract IST #04170) is acknowledged.

References

[1] N. Izuka, K. Kaneko, and N. Suzuki, IEEE J. Quantum Electron. **42**, 765 (2006).
[2] F. R. Giorgetta, E. Baumann, F. Guillot, E. Monroy, and D. Hofstetter, Electron. Lett. **43**, 185 (2007).
[3] L. Nevou, M. Tchernycheva, F. H. Julien, F. Guillot, and E. Monroy, Appl. Phys. Lett. **90**, 121106 (2007).
[4] M. Tchernycheva, L. Nevou, L. Doyennette, F. H. Julien, F. Guillot, E. Monroy, T. Remmele, and M. Albrecht, Appl. Phys. Lett. **88**, 153113 (2006).
[5] P. Holmström, IEEE J. Quantum Electron. **42**, 8 (2006).
[6] D. Hofstetter, E. Baumann, F. R. Giorgetta, M. Graf, M. Maier, F. Guillot, E. Bellet-Amalric, and E. Monroy, Appl. Phys. Lett. **88**, 121112 (2006).
[7] L. Nevou, N. Kheirodin, and M. Tchernycheva, Appl. Phys. Lett. **90**, 223511 (2007).